Bone 120 (2019) 297–304

Contents lists available at ScienceDirect

Bone

journal homepage: www.elsevier.com/locate/bone

Full Length Article

Innervation of the tibial epiphysis through the intercondylar foramen

Koichi Matsuo[a,*], Shuting Ji[a], Ayako Miya[a], Masaki Yoda[a], Yuzuru Hamada[b], Tomoya Tanaka[c], Ryoko Takao-Kawabata[c], Katsuhiro Kawaai[a], Yukiko Kuroda[a], Shinsuke Shibata[d]

[a] Laboratory of Cell and Tissue Biology, Keio University School of Medicine, 35 Shinanomachi, Shinjuku-ku, Tokyo 160-8582, Japan
[b] Morphology Section, Primate Research Institute, Kyoto University, 41 Kanrin, Inuyama 484-8506, Japan
[c] Pharmaceuticals Research Center, Asahi Kasei Pharma Corporation, 632-1 Mifuku, Izunokuni, Shizuoka 410-2321, Japan
[d] Electron Microscope Laboratory, Keio University School of Medicine, 35 Shinanomachi, Shinjuku-ku, Tokyo 160-8582, Japan

ARTICLE INFO

Keywords:
Epiphysis
Knee joint
Tibia
Foramen
Sensory neuron
Schwann cells

ABSTRACT

The periosteum and mineralized bone are innervated by nerves that sense pain. These include both myelinated and unmyelinated neurons with either free nerve endings or bearing nociceptors. Parasympathetic and sympathetic autonomic nerves also innervate bone. However, little is known about the route sensory nerves take leaving the epiphyses of long bones at the adult knee joint. Here, we used transgenic mice that express fluorescent Venus protein in Schwann cells (*Sox10*-Venus mice) to visualize myelinated and unmyelinated nerves in the tibial epiphysis. Immunofluorescence to detect a pan-neuronal marker and the sensory neuron markers calcitonin gene-related peptide (CGRP) and tropomyosin receptor kinase A (TrkA) also revealed Schwann cell-associated sensory neurons. Foramina in the intercondylar area of the tibia were conserved between rodents and primates. Venus-labeled fibers were detected within bone marrow of the proximal epiphysis, exited through foramina along with blood vessels in the intercondylar area of the tibia, and joined Venus-labeled fibers of the synovial membrane and meniscus. These data suggest that innervation of the subchondral plate and trabecular bone within the tibial epiphysis carries pain signals from the knee joint to the brain through intercondylar foramina.

1. Introduction

Both myelinated and unmyelinated nerve fibers innervate the skeleton. Pain sensation and bone mass regulation are two extensively studied functions of these fibers in the adult skeleton [1]. Bone pain is associated with pathologies such as bone metastasis of malignant tumors, bone fracture, and, in the elderly, osteoarthritis. Bone pain-sensing nociceptors include both thinly myelinated Aδ fibers and smaller-diameter unmyelinated C fibers [2]. Neurons of both types express calcitonin gene-related peptide (CGRP) and tropomyosin receptor kinase A (TrkA), the latter a high affinity receptor for nerve growth factor (NGF). Internalized NGF-TrkA complexes are transported to the dorsal root ganglia (DRG) where they increase expression of genes encoding CGRP and other neuropeptides, thereby increasing pain sensitivity. Non-pain sensing proprioceptors and mechanoreceptors are also localized within long bones. The periosteum on the bone surface is more densely innervated with sensory nerves than are bone marrow and mineralized bone [3]. CGRP also mediates bone pain induced by fungal infection and suppresses osteoinflammation [4]. The skeleton is also significantly innervated by the autonomic nervous system, including both adrenergic and cholinergic sympathetic nerve fibers [5]. Sympathetic nerves modulate vascular tonus and pain sensing and regulate bone remodeling by suppressing osteoblastic bone formation and enhancing osteoclastic bone resorption [6,7].

The tibia is the second largest weight-bearing bone after the femur in mice and other mammals. The tibia is enveloped by the periosteum, and the epiphysis develops at the secondary ossification center sandwiched between articular cartilage and the growth plate. The knee joint, which is covered by the synovial membrane, is a major site of bone pain in osteoarthritis. Sensory nerves at the knee joint are the target of analgesic or pain-relieving treatments, and stimulation of epiphyseal sensory nerves contributes to knee pain. Within the knee joint, between the femur and tibia are two C-shaped fibrocartilages called menisci, which when torn result in knee pain. Epiphyseal sensory and autonomic innervation has been studied mostly in rat in developing long bones at the knee joint [8,9]. However, the route taken by sensory nerves as they leave epiphyses at the adult knee joint remains unclear.

In mammals, Schwann cells are derived from neural crest cells and express the transcription factor Sox10 at all stages of differentiation [10]. To track Schwann cells, we previously generated mice expressing Venus, a

* Corresponding author at: Keio University School of Medicine, Shinanomachi 35, Shinjuku-ku, Tokyo 160-8582, Japan.
E-mail address: kmatsuo@keio.jp (K. Matsuo).

https://doi.org/10.1016/j.bone.2018.11.007
Received 16 May 2018; Received in revised form 9 November 2018; Accepted 12 November 2018
Available online 13 November 2018

bright version of green fluorescent protein (GFP), under control of the *Sox10* promoter and reported Venus expression in neural crest cells and in both myelinating and non-myelinating Schwann cells [11]. Schwann cells are associated with myelinated and unmyelinated peripheral nerve axons, the former wrapped multiple times by the myelin sheath and the latter in close association with Schwann cells [12].

In this study, we used *Sox10*-Venus transgenic mice to trace both myelinated and unmyelinated nerve bundles and determine how they entered into the proximal epiphysis of tibia. Using this approach combined with marker analysis, we detected extensive sensory innervation of the proximal tibial epiphysis through foramen(-ina) between the two condyles.

2. Materials and methods

2.1. Animals and human subjects

Establishment of the *Sox10*-Venus transgenic mouse strain was reported previously [11]. Adult mice (1.5-, 3-, 5-, 6-, 7-, 9-, 10-, 12-, and 14-months-old; a total of > 48) were anesthetized and sacrificed by transcardial perfusion or cervical dislocation. Both left and right legs were analyzed. Experimental protocols were approved by the Keio University Institutional Animal Care and Use Committee.

For micro-CT analyses, isolated hind limbs of Sprague-Dawley rats (Japan SLC) were used. Experimental protocols were approved by the Experimental Animal Ethics Committee at Asahi Kasei Pharma Corp.

Isolated dried tibiae of male Japanese macaques (*Macaca fuscata fuscata*, $n = 9$) from the collection at the Primate Research Institute, Kyoto University, were also used. The research protocol was approved by the Animal Welfare and Animal Care Committee, Primate Research Institute, Kyoto University. All animal experiments were carried out in accordance with Institutional Guidelines on Animal Experimentation. Human proximal tibiae were isolated from a formalin-embalmed cadaver (female, 97 years old) in accordance with the Declaration of Helsinki. The procedure had been approved by the Institutional Review Board at Keio University School of Medicine.

2.2. Lightsheet microscopy

Mice were deeply anesthetized and transcardially perfused with phosphate-buffered saline (PBS) containing 10 U/ml heparin followed by 4% paraformaldehyde (PFA) in PBS. Tibiae were decalcified in 10% EDTA in 0.1 M Tris (final pH 7) for 2 weeks at 4 °C on a rotator. Samples were washed in PBS and then cleared using CUBIC-L solution (T3740, Tokyo Chemical Industry) at 37 °C for 4 days on a shaker (70 rpm) [13]. CUBIC-L solution was removed and samples were washed in 0.1 M phosphate buffer containing 0.5 M NaCl, and then incubated in 1:1 water-diluted CUBIC-R + (T3741, Tokyo Chemical Industry) solution at 37 °C for 1 day and then undiluted CUBIC-R + for 2 days on a shaker (70 rpm). Samples were then stored at room temperature until observation. For analysis, samples were transferred to acrylic tubes filled with CUBIC-R + and sealed with plastic paraffin film, which were then hung in a chamber filled with silicone oil AR20 (10,836, SIGMA-Aldrich) and analyzed by lightsheet microscopy (Lightsheet Z.1, Carl Zeiss). Approximately 100 slices were obtained at 488 nm excitation with a 5× dry lens (1.372 μm/pixel, 1920 × 1920). *Z*-projection images were generated using IMARIS software (Bitplane).

2.3. Fluorescence stereo microscopy

Fluorescence stereo microscopes (Leica M205FA and Nikon SMZ25) were used with a Leica GFP filter (Excitation 545 nm/30, Emission 620 nm/60 BP) and a Nikon P2-EFL GFP-L Filter Cube.

2.4. Histology

For lectin perfusion, anesthetized mice were lightly sedated by intraperitoneal (IP) injections of a mix of medetomidine (0.3 mg/kg), dormicum (4 mg/kg) and butorphanol tartrate (5 mg/kg) and then injected through the proximal tail vein with 1 mg/ml DyLight 594 *Lycopersicon esculentum* (TOMATO) LECTIN (DL-1177, Vector Laboratories) using a 30-G needle. Thirty minutes later, mice were re-anesthetized and perfused through the heart using a syringe pump (KDS100, Muromachi Kikai) connected to a 26-G needle, set at a pumping rate of 0.41 ml/min. Perfusion fluids included 10 ml of 10 units/ml heparin followed by 10 ml of 4% PFA in PBS. After perfusion tissues were dissected, fixed at 4 °C in 4% PFA in PBS overnight on a rotator, and frozen in preparation for sectioning.

For immunofluorescence, frozen 10 μm sections were generated using Kawamoto's film method [14]. We used rabbit anti-CGRP polyclonal antibody (CA1134, BIOMOL, 1:500), rabbit anti-TrkA polyclonal antibody (06-574, Merck, 1:100), rat anti-GFP monoclonal antibody (GF090R, Nacalai, 1:1000), hamster anti-CD31 monoclonal antibody (MAB1398Z) and rabbit and rat normal IgG (SIGMA-Aldrich) and hamster normal IgG (ab18479, abcam) as primary antibodies, and Alexa568-conjugated goat anti-rabbit IgG (A-11036, Invitrogen, 1:500), Alexa594-conjugated donkey anti-rabbit IgG (ab150068, abcam, 1:500), Alexa594-conjugated goat anti-rat IgG (A-11007, Invitrogen, 1:500), Alexa647-conjugated goat anti-rat IgG (A-21247, Invitrogen, 1:500), Alexa488-conjugated donkey anti-rat IgG (A-21208, Invitrogen, 1:1000), and biotin-conjugated goat anti-hamster IgG (405,501, BioLegend) with Alexa647-conjugated Avidin as secondary antibodies. Nuclei were stained with 1 μg/ml DAPI (SIGMA-Aldrich). Sections were analyzed by confocal laser scanning microscopy (Zeiss LSM710, Olympus FV3000). For serial cross sections, samples were decalcified and embedded in a reagent used to prepare frozen sections, 30 slices at 50 μm intervals (total thickness, 1.5 mm) (FSC 22, Leica).

2.5. Whole-mount staining

Isolated tibiae were cut at the diaphysis, and proximal halves were fixed overnight in 4% PFA/PBS at 4 °C. A part of the proximal epiphysis was removed manually using a 76 μm thick-blade (76 Cutting Blade, Nisshin EM). Samples were incubated in 0.3% Triton X-100/PBS at RT for 10 min. After blocking, samples were stained with rabbit Neuro-Chrom Cy3-conjugated anti-pan neuronal marker antibody (ABN2300C3, Millipore, 1: 50) and 2 μg/ml DAPI (SIGMA-Aldrich). Samples were analyzed using a confocal laser scanning microscope (Zeiss LSM710).

2.6. Micro-CT analysis

For phosphotungstic acid (PTA) staining, mice were dissected and, after removal of skin and most muscles, lower legs were fixed in 4% PFA/1% glutaraldehyde (4F1G) in PBS overnight at 4 °C on a rotator. After washing first in PBS and then in H_2O, the sample was placed on a rotator and immersed once in 35% ethanol for 15 min at 4 °C, twice in 70% ethanol for 15 min at 4 °C, and then in 0.3% PTA in 70% ethanol for 12 days at 4 °C [15]. The sample was washed in 70% ethanol, and CT imaging was performed in 70% ethanol using the R_mCT2 system (Rigaku) at a field of view of 5 mm (isotropic voxel size,10 μm), as previously described [16]. Distal tibia was fixed in 70% ethanol overnight at 4 °C on a rotator and air-dried.

Isolated hind limbs of Sprague-Dawley rats were imaged using a cone-beam X-ray micro-CT system (ScanXmate-RB090SS150; Comscantechno, Kanagawa, Japan), which was operated at 70 kV, 100 μA, and an isotropic voxel size of 28.5 or 76.2 μm. Isolated tibiae from Japanese macaques or from human cadavers were imaged using the R_mCT2 system (Rigaku) at a field of view of 30 mm (isotropic voxel size, 60 μm). 3D images were analyzed using TRI/3D-Bon (RATOC System Engineering) and ImageJ (NIH) software.

3. Results

To visualize Schwann cells inside the tibia, we assessed tibiae from adult *Sox10*-Venus mice using fluorescence stereo microscopy. As expected, the periosteum showed an enriched network of *Sox10*-Venus-positive cells (Supplemental Fig. S1A, arrows). We next decalcified tibiae and treated them with tissue-clearing reagents in preparation for lightsheet microscopy [13]. Analysis of the proximal epiphysis revealed *Sox10*-Venus-positive cells that extended to the synovial space (Fig. 1A). We then asked whether these Venus-positive cells were in the marrow of the tibial epiphysis. After removing the articular surface, which was cut parallel to the tibial growth plate (Fig. 1B, line), we observed a network of *Sox10*-Venus-positive cells mainly in the bone marrow of the epiphysis (Fig. 1C, D). Maximum Intensity Projection (MIP) images of epiphysis revealed Schwann cell networks (Fig. 1E). Serial cross sections of the epiphysis and growth plate revealed that abundant epiphyseal *Sox10*-positive fibers traveled within the epiphysis but did not enter the growth plate. (Fig. 1F, Supplemental Fig. S1B–G). All *Sox10*-Venus-positive signals were also GFP-positive, and analysis with an anti-GFP antibody was helpful to detect small fibrous structures in epiphyseal bone marrow (Supplemental Fig. S2). These data suggest that Schwann cells are abundant in the proximal epiphysis of the tibia.

To confirm whether *Sox10*-Venus-positive cells are associated with nerve fibers, we first performed whole-mount immunostaining of the tibial epiphysis (Fig. 2A). Venus-positive cells (Fig. 2B) closely co-localized with distinct linear structures likely to be nerve axons, as they were marked by the Neuro-Chrom pan-neuronal marker (Fig. 2C, D). We then assessed staining for the sensory neuron marker CGRP in a frozen section of the tibial epiphysis (Fig. 2E). At high magnification, we detected Venus-positive cells (Fig. 2F) associated with CGRP-

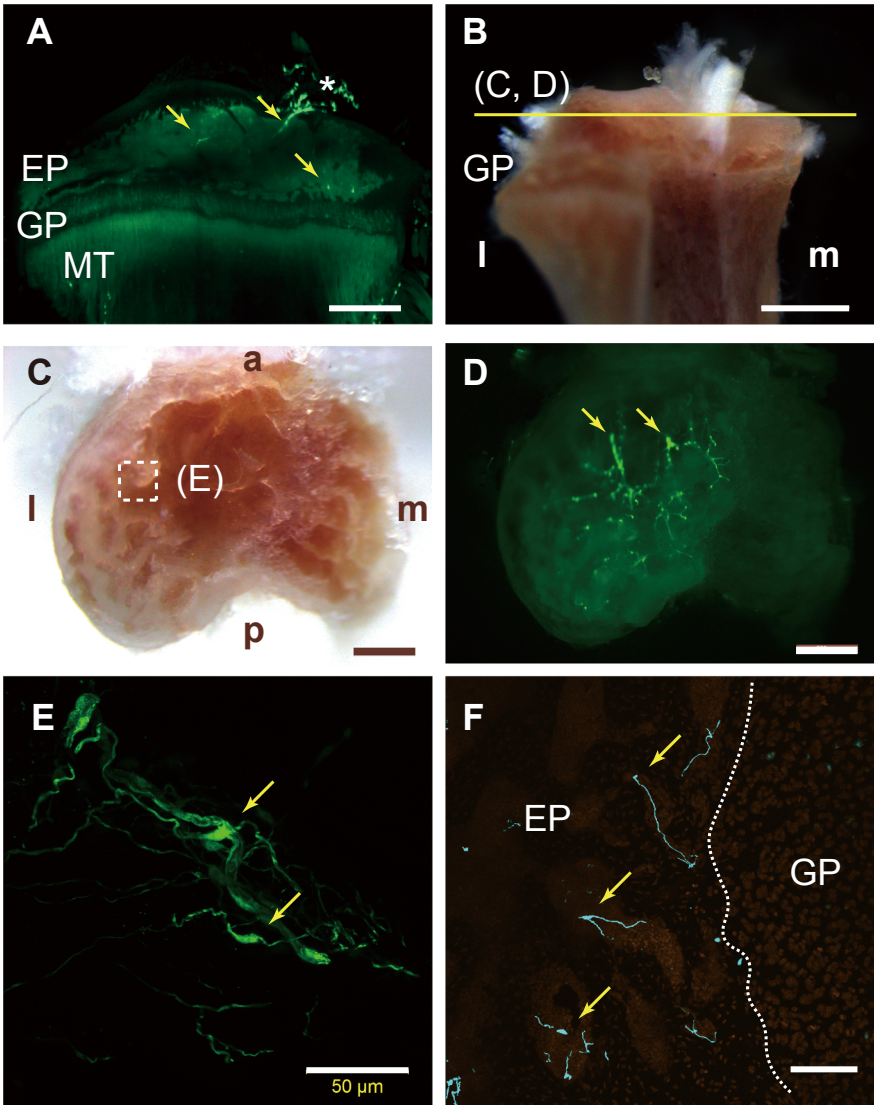

Fig. 1. *Sox10*-Venus-positive Schwann cells in the tibial epiphysis. (A) Lightsheet microscopy of pseudo-left tibia (right tibia was flipped *in silico*) isolated from a 6-week-old male *Sox10*-Venus mouse. Posterior view of the mid anteroposterior plane, as visualized by *Z*-projection images. Arrows, *Sox10*-Venus-expression in the epiphysis. Asterisk, an extension of *Sox10*-positive cells to the synovial space. EP, epiphysis; GP, growth plate; MT, metaphysis. Scale bar, 500 μm. (B) Posterior view of left tibia of a 3-month-old male mouse. Horizontal yellow line indicates cutting surface of (C, D). l, lateral. m, medial. Scale bar, 1 mm. (C) Top view of a horizontally-cut epiphysis of the left tibia from a 12-month-old female *Sox10*-Venus mouse taken on a stereo microscope. Scale bar, 500 μm. Dotted square indicates approximate area shown in (E). (D) *Sox10*-Venus-positive cells (arrows) in the horizontally-cut epiphysis. Scale bar, 500 μm. (E) MIP image of horizontally-cut epiphysis of a 14-month-old male mouse. Image is generated using a 10× objective and from 24 slices at 3-μm intervals (total thickness, 69 μm). Higher magnification of boxed area in (C). Image was acquired using a 40× objective and assembled from 13 slices at 3 μm intervals (total thickness, 36 μm). Scale bar, 50 μm. (F) Proximal tibial EP-GP boundary in a 2-month-old male mouse ($n = 2$). Image was acquired using a 40× objective and assembled from 31 slices at 1 μm intervals (total thickness, 30 μm). Scale bar, 100 μm. (For interpretation of the references to colour in this figure legend, the reader is referred to the web version of this article.)

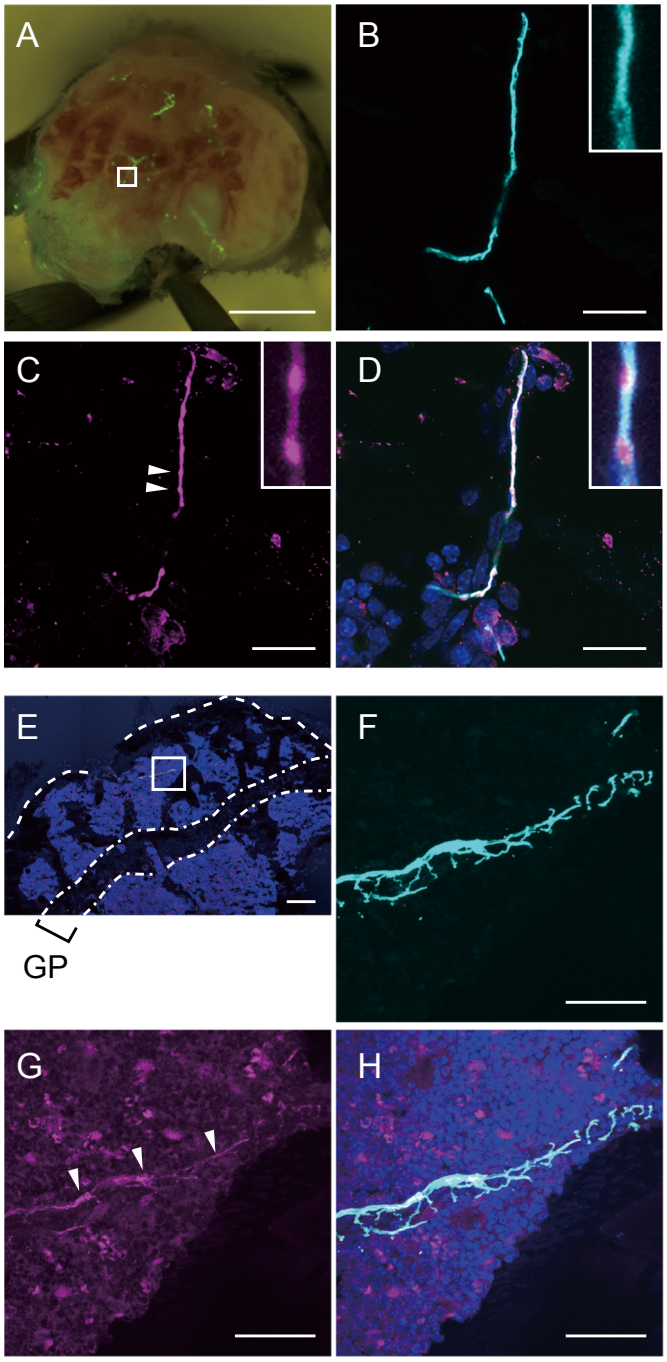

Fig. 2. Co-localization of Schwann cells with CGRP-positive neurons in the tibial epiphysis. (A) Horizontal section of tibial epiphysis in a 6-month-old male mouse (n = 2). Scale bar, 1 mm. Boxed area is analyzed by confocal microscopy in (B)-(D) with magnified views (insets). (B) *Sox10*-Venus-positive lines representing Schwann cells. (C) Staining of the sample in (B) with the pan-neuronal marker Neuro-Chrom. Arrowhead, node of Ranvier. (D) Merge of (B), (C) and DAPI staining. Scale bars, 20 μm. (E) Sagittal section of tibial epiphysis in a 7-month-old male mouse (n = 2). GP, growth plate. Scale bar, 200 μm. Boxed area is analyzed by confocal microscopy in (F)-(H). (F) A *Sox10*-Venus-positive network of Schwann cells. (G) CGRP-positive axons (arrowheads). (H) Merged image of (F), (G) and DAPI. Scale bars, 50 μm.

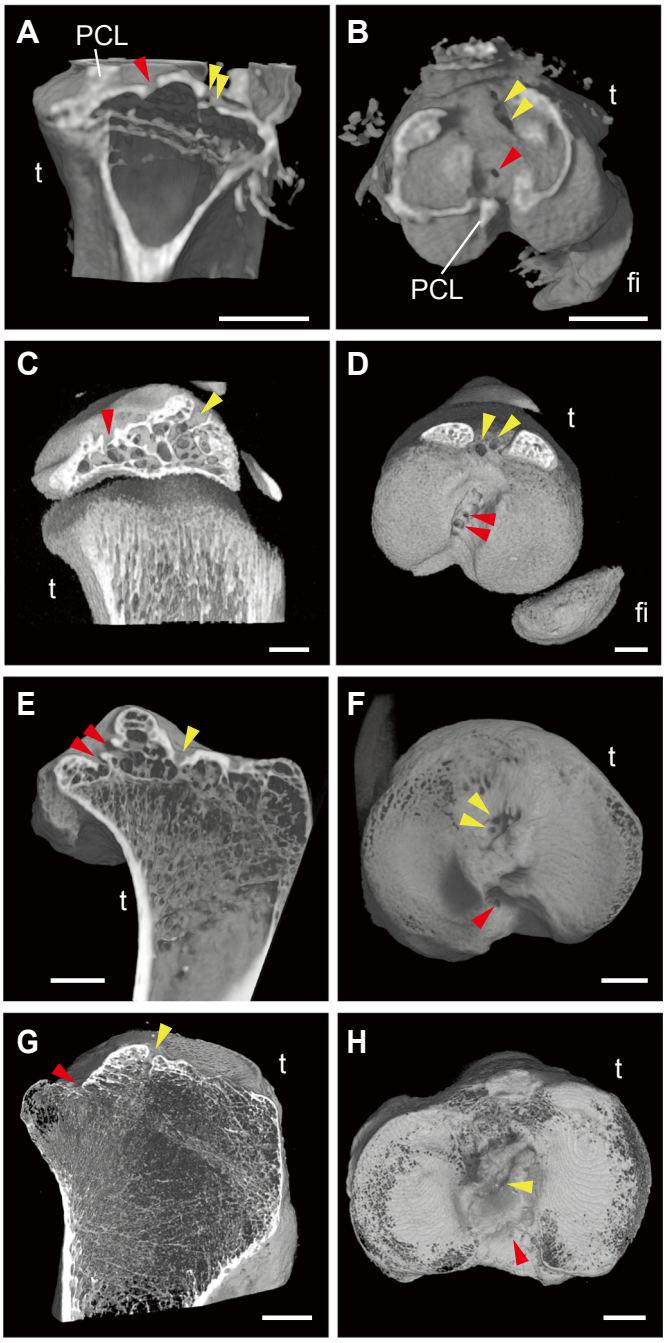

Fig. 3. CT images of intercondylar foramina in the tibial proximal epiphysis. (A, B) PTA-stained right knee joint of a 9-month-old female mouse (n = 2). t, tibia. fi, fibula PCL, posterior cruciate ligament. Arrowheads, anterior (yellow) and posterior (red) intercondylar foramina. Scale bars, 1 mm. (C, D) Unstained right knee joint of 6-week-old male rat. Scale bars, 1 mm. (E, F) Unstained right tibia of a 6-year-old male Japanese macaque (n = 4). Scale bars, 5 mm. (G, H) Unstained right tibia of a 97-year-old human female. Scale bars, 10 mm. (A), (C), (E) and (G), Lateral view, anterior is towards right (lateral part of the tibia was removed *in silico*). (B), (D), (F) and (H), Superior view, anterior is towards top. Femurs were removed in (B) and (D) *in silico*. (For interpretation of the references to colour in this figure legend, the reader is referred to the web version of this article.)

positive neurons (Fig. 2G,H), suggesting that sensory axons innervate the tibia epiphysis.

The mammalian epiphysis is largely encased by articular cartilage and cortical bone, and fibers in neuronal networks must exit the epiphysis to travel to the central nervous system. To search for that exit in mouse, we examined the tibial epiphysis using micro-CT. Proximal tibia stained with the soft tissue contrast agent phosphotungstic acid (PTA) exhibited foramina between condyles connecting epiphyseal bone marrow to the synovial space (Fig. 3A). Fig. 3B shows a superior view from the knee joint, clearly revealing foramina, including one near the

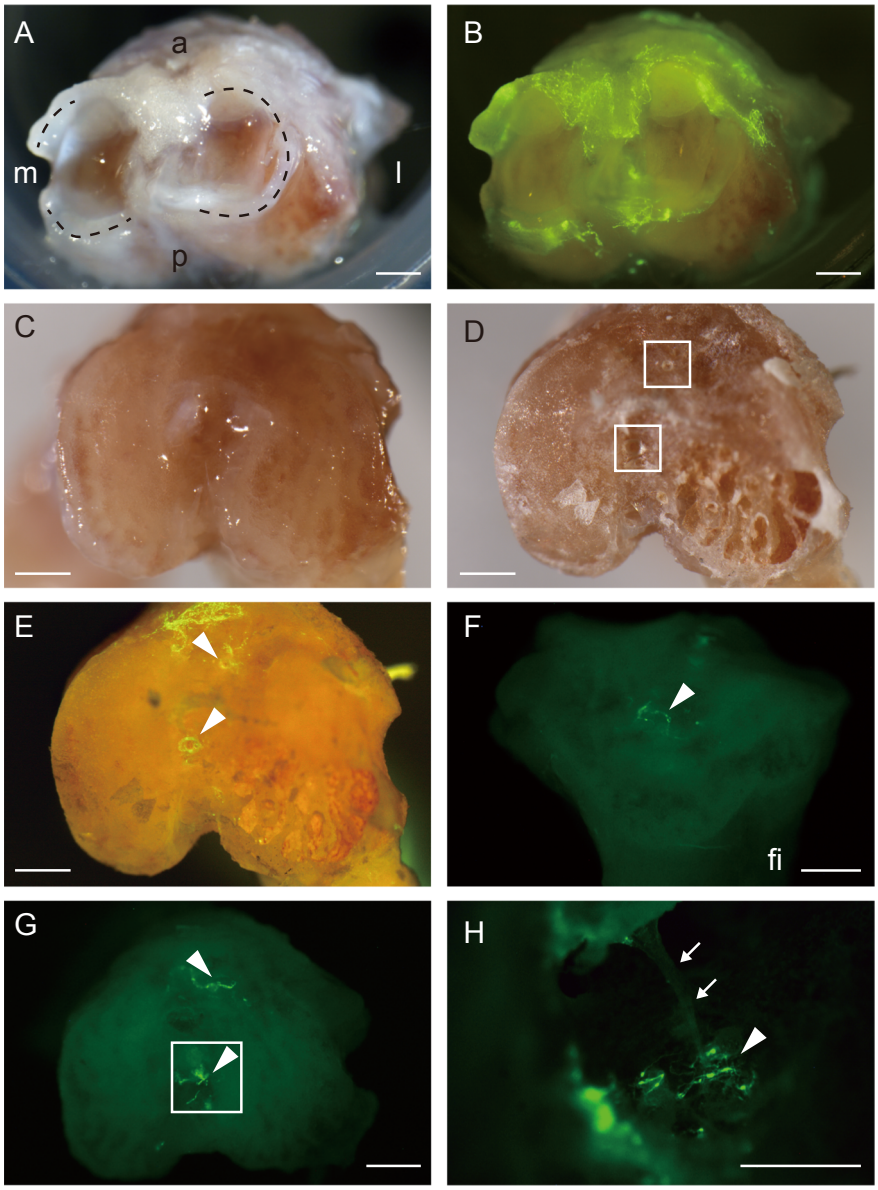

Fig. 4. *Sox10*-Venus-positive Schwann cells pass through intercondylar foramina of the proximal tibial epiphysis in mouse. (A) Proximal right tibia with synovial membranes around menisci from a 10-month-old female mouse. Dotted lines, menisci. a, anterior. p, posterior. m, medial. l, lateral. (B) *Sox10*-Venus-positive signals in sample shown in (A). (C) Superior view of articular surface of the tibia from 12-month-old male mouse. (D) Intercondylar foramina (boxes) revealed after removal of articular cartilage shown in (C). (E) *Sox10*-Venus-positive cells around foramina (arrowheads) in (D). (F) Posterior view of the right tibia from a 7-month-old female. *Sox10*-Venus-positive cells are visible in the intercondylar foramen (arrowhead). fi, fibula. (G) Superior view of the tibia shown in (F). Arrowheads indicate intercondylar foramina. (H) Trabecular bone (arrows) within the foramen associated with *Sox10*-Venus-positive cells (arrowhead) shown in (G, box). Scale bars, (A)–(G) 500 μm, (H) 200 μm.

posterior cruciate ligament (PCL). Similar intercondylar foramina were readily observable in rat knee (Fig. 3C, D) and in tibiae of Japanese macaques (Fig. 3E, F) and humans (Fig. 3G, H). These data suggest the presence of intercondylar foramina in a wide range of mammalian species.

We next asked whether Venus-labeled fibers in *Sox10*-Venus mice pass through the intercondylar foramen by evaluating fluorescent signals of Schwann cells contained in nerve bundles in *Sox10*-Venus mice. To do so, we first removed the femur and exposed the articular surface of the knee joint. Analysis by fluorescence stereo microscopy revealed abundant *Sox10*-Venus-positive cells in lateral and medial menisci (Fig. 4A, B). We then removed the menisci and synovial membrane (Fig. 4C) and further scraped off the articular surface and subchondral plate of tibia. As expected, we observed foramina edged with *Sox10*-Venus-positive cells located in the intercondylar region (Fig. 4D, E). We observed co-localization of the intercondylar foramen and Venus-positive cells in every tibia examined (Fig. 4F, G). Venus-positive fibers associated with trabecular bone were also visible inside the foramen (Fig. 4H). These data indicate that fibers containing Venus-labeled Schwann cells pass through intercondylar foramina in the tibia.

We next asked whether neural foramina exist in the distal epiphysis of the tibia. MicroCT analysis revealed foramina at anterior and medial epiphyseal external surfaces of the distal tibia in mice (Supplemental Fig. S3, A–D). We detected Venus expression at an anterior foramen in *Sox10*-Venus mice, indicative of a neural foramen (Supplemental Fig. S3, E–G). We also observed epiphyseal foramina at anterior and medial external surfaces of the distal tibia in rats (Supplemental Fig. S3, H–K). On the other hand, Japanese macaques showed foramina on the medial articular surface of the epiphysis (Supplemental Fig. S3, L and O) in addition to anterior and medial external surfaces (Supplemental Fig. S3,

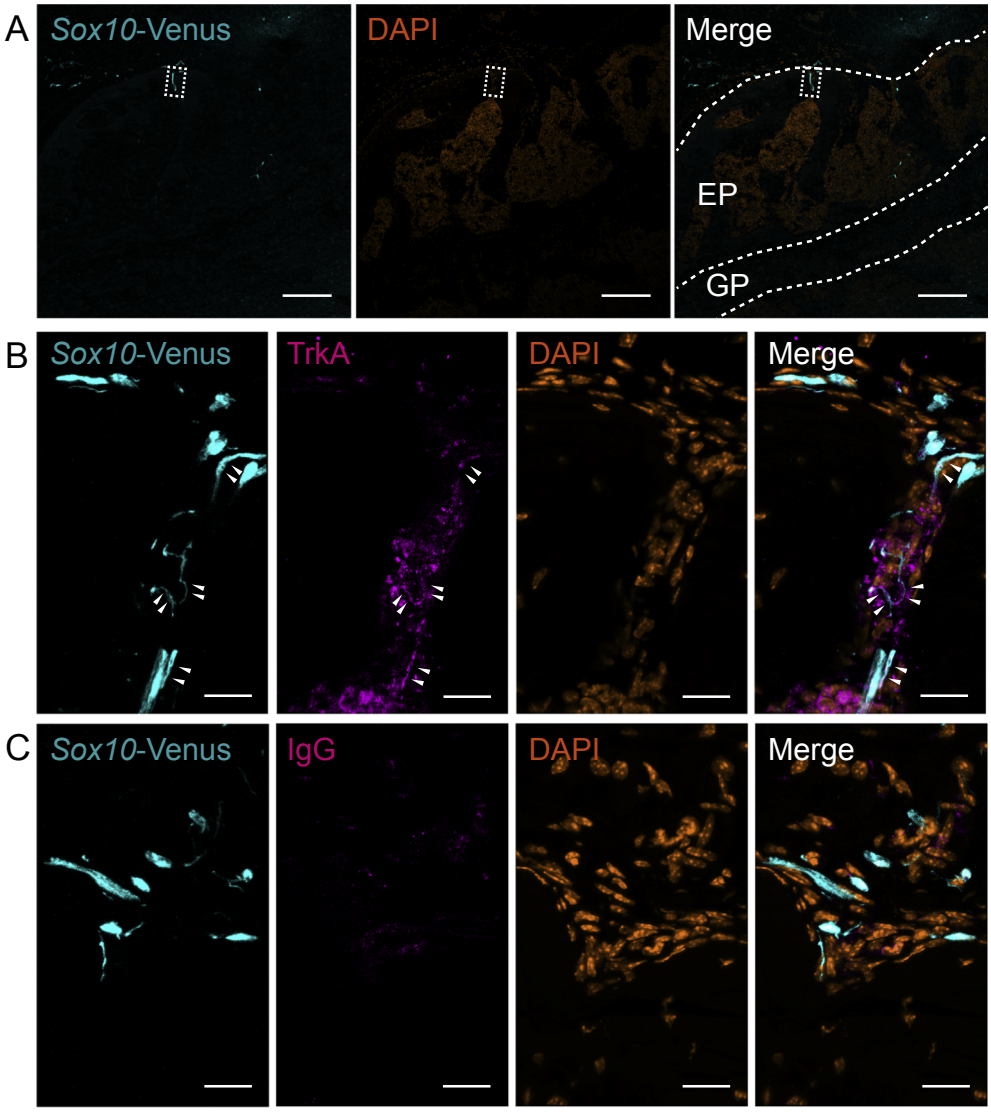

Fig. 5. Association of Schwann cells with TrkA-positive neurons in the tibial intercondylar foramen. (A) Longitudinal section of the tibial epiphysis in an 8-month-old male mouse (n = 2). Scale bars, 200 μm. Boxed area is analyzed by confocal microscopy in (B)–(C). EP, epiphysis; GP, growth plate. (B) *Sox10*-Venus-positive and TrkA-positive signals (arrowheads). Scale bars, 20 μm. (C) IgG control. Scale bars, 20 μm.

M and N). These data suggest that neural foramina are located at the epiphyses of long bones beyond species.

During endochondral ossification, NGF-TrkA signaling by sensory nerves coordinates vascularization with ossification [17]. We therefore asked whether TrkA and *Sox10*-Venus expression co-localize at the intercondylar foramen (Fig. 5A). Nerves visualized by anti-TrkA antibody were closely associated with *Sox10*-Venus-positive structures (Fig. 5B, C), suggesting that TrkA-expressing sensory neurons pass through the intercondylar foramen.

Finally, we analyzed possible association of sensory fibers with blood vessels in the tibial epiphysis. Perfusion of *Sox10*-Venus mice with fluorochrome-labeled tomato lectin, which binds to the internal surface of blood vessels, revealed that *Sox10*-Venus-positive structures were closely associated with blood vessels at the intercondylar foramen of the proximal tibia (Fig. 6A). As expected, CD31-positive endothelial cells largely overlapped with tomato lectin-labeled blood vessels (Fig. 6A, B). In cross-sections of blood vessels at the intercondylar foramen, *Sox10*-Venus-positive cells and their thin fibers were associated with blood vessels (Fig. 6C). These data indicate that blood vessels are present in close proximity with cells expressing *Sox10*-Venus in the tibial epiphysis.

4. Discussion

In this study, we focused on the tibial proximal epiphysis and found that the subchondral plate and trabecular bone within the epiphysis is innervated by sensory nerves, based on the close association between Schwann cells and cells positive for a pan-neuronal marker or for CGRP or TrkA. These nerves left the tibial epiphysis through intercondylar foramina and likely contribute to sensations of pain in the knee.

Afferent nerve fibers carrying sensory information from the subchondral plate and trabecular bone within the epiphysis pass through evolutionally conserved intercondylar foramina, at least in mice, rats, macaques and humans, into the knee joint. Intercondylar foramina face the synovial membrane and are in the vicinity of cruciate ligaments. PCL are less vulnerable to injury compared with the anterior cruciate ligament (ACL) [18]. Mouse models representing various stages of osteoarthritis have been created through a combination of ligament transection and menisectomy [19]. In these models, epiphysis-derived sensory nerves are likely to be injured and participate in the pathology. Retrograde tracing experiments from the distal femoral epiphysis or distal tibial epiphysis in rat pups has revealed labeling primarily in L2-L5 DRG, and 31–33% of labeled DRG neurons were reportedly CGRP-

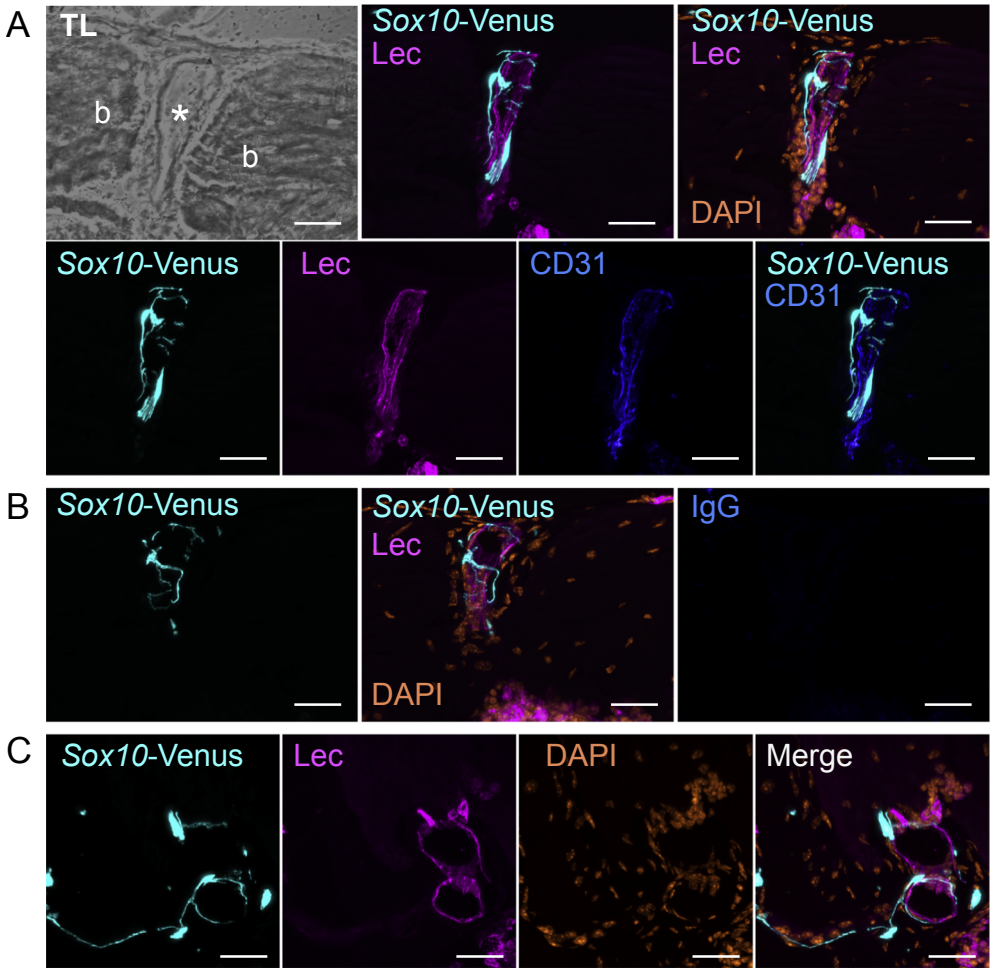

Fig. 6. Association of Schwann cells with CD31-positive blood vessels in the tibial intercondylar foramen. (A) Transmission light microscopy (TL) showing a longitudinal cut of a frozen section of tibial epiphysis in a 2-month-old male mouse ($n = 2$). Scale bar, 30 μm. Asterisk indicates intercondylar foramen between bone (b). Fluorescence *Z*-projection detection of *Sox10*-Venus, tomato-lectin-labeled blood vessels (Lec), CD31-positive endothelial cells, and nuclei (DAPI). Scale bars, 30 μm. (B) IgG control for the CD31 antibody. (C) A different field showing association between *Sox10*-Venus-positive Schwann cells and tomato-lectin-labeled endothelial cells (Lec) in cross-sections of blood vessels at an intercondylar foramen of the proximal tibia. Scale bars, 30 μm.

positive [20,21], suggesting that sensory inputs from the proximal tibial epiphysis likely reach the DRG. In humans, knee pain is particularly associated with osteoarthritis in the elderly. A limitation of this study is that the sample size was too small to allow comparisons between age groups. However, this study should shed light on the organization of sensory nerves in the epiphysis in the context of human diseases.

The lateral and medial articular surfaces of the tibia are covered by cartilage, while the intercondylar region is cartilage-free and provides attachment sites for menisci, synovial membranes, and cruciate ligaments. In this context, intercondylar foramina are located close to but outside of articular surfaces. This anatomy may exquisitely position foramina to serve as exits for nerves from the epiphyses of long bones other than tibia. The intercondylar fossa of the distal femur is perforated and harbors vascular foramina in humans [22]. Co-patterning of the vascular and neuronal system is well documented: for example, migrating neurons in the CNS use blood vessels as scaffolds, and in the PNS sensory neurons and Schwann cells provide a template for patterning of arteries [23,24]. We show that cells expressing *Sox10*-Venus are associated with blood vessels at intercondylar foramina in adult mice (Fig. 6). While Sox10-positive cells reportedly differentiate into vascular mural cells [25], we conclude that *Sox10*-Venus cells in intercondylar foramina are Schwann cells, as they co-localized with cells positive for neuronal markers (Fig. 2, Fig. 5). These data suggest that vascular foramina also act as neural foramina in the tibial epiphysis.

Secondary ossification centers at the epiphysis, which require vascularization and innervation, were likely acquired during mammalian evolution [26]. Blood vessels are crucial for endochondral ossification [27,28], and Tomlinson et al. reported that sensory neurons coordinate vascularization with ossification in long bones [17]. Curiously, they observed that nerves from the epiphyseal surface enter and inhabit epiphyseal vascular canals. Indeed, TrkA signaling is required for formation of secondary ossification centers in the developing femur [17].

Studies in mouse indicate that once bones develop, sensory nerves are required for skeletal adaptation to mechanical loads by increasing load-induced bone formation [29,30]. Furthermore, CGRP inhibits osteoclast activity and bone resorption [31,32], and others have reported involvement of CGRP-containing nerve fibers in bone remodeling [33,34]. CGRP and TrkA nociceptive markers are upregulated in neurons innervating the subchondral bone in a rat osteoarthritis model [35], and the density of synovial CGRP-positive nerve fibers is reportedly lower in rheumatoid arthritis than in osteoarthritis patients [36]. However, the functional significance of sensory nerves in tibial and femoral epiphyses in knee pathologies remains unclear.

In summary, we demonstrate innervation of the subchondral bone plate and trabecular bone in the epiphysis. Besides pain sensing, epiphyseal sensory neurons may function in maintenance of subchondral bone. This matter should be further investigated as relevant to pharmaceutical and surgical intervention of the knee joint.

Supplementary data to this article can be found online at https://doi.org/10.1016/j.bone.2018.11.007.

Acknowledgments

We thank Ayako Sakamoto and Kazumasa Takenouchi for help with immunohistochemistry, and Makoto Morikawa for help with CT imaging of monkey bones. We also thank the Clinical Anatomy Laboratory at Keio University School of Medicine for preparation and dissection of an embalmed cadaver, and the Collaborative Research Resources at Keio University School of Medicine for technical assistance. This study was funded by Asahi Kasei Pharma Corporation and JSPS KAKENHI Grant Number 17H04015.

References

[1] S. Nencini, J.J. Ivanusic, The physiology of bone pain. How much do we really know? Front. Physiol. 7 (2016) 157.
[2] P.W. Mantyh, M. Koltzenburg, L.M. Mendell, L. Tive, D.L. Shelton, Antagonism of nerve growth factor-TrkA signaling and the relief of pain, Anesthesiology 115 (2011) 189–204.
[3] P.W. Mantyh, The neurobiology of skeletal pain, Eur. J. Neurosci. 39 (2014) 508–519.
[4] K. Maruyama, Y. Takayama, T. Kondo, K.I. Ishibashi, B.R. Sahoo, H. Kanemaru, Y. Kumagai, M.M. Martino, H. Tanaka, N. Ohno, Y. Iwakura, N. Takemura, M. Tominaga, S. Akira, Nociceptors boost the resolution of fungal osteoinflammation via the TRP channel-CGRP-Jdp2 Axis, Cell Rep. 19 (2017) 2730–2742.
[5] D.B. Mach, S.D. Rogers, M.C. Sabino, N.M. Luger, M.J. Schwei, J.D. Pomonis, C.P. Keyser, D.R. Clohisy, D.J. Adams, P. O'Leary, P.W. Mantyh, Origins of skeletal pain: sensory and sympathetic innervation of the mouse femur, Neuroscience 113 (2002) 155–166.
[6] S. Takeda, F. Elefteriou, R. Levasseur, X. Liu, L. Zhao, K.L. Parker, D. Armstrong, P. Ducy, G. Karsenty, Leptin regulates bone formation via the sympathetic nervous system, Cell 111 (2002) 305–317.
[7] F. Elefteriou, J.D. Ahn, S. Takeda, M. Starbuck, X. Yang, X. Liu, H. Kondo, W.G. Richards, T.W. Bannon, M. Noda, K. Clement, C. Vaisse, G. Karsenty, Leptin regulation of bone resorption by the sympathetic nervous system and CART, Nature 434 (2005) 514–520.
[8] F. Hara-Irie, N. Amizuka, H. Ozawa, Immunohistochemical and ultrastructural localization of CGRP-positive nerve fibers at the epiphyseal trabecules facing the growth plate of rat femurs, Bone 18 (1996) 29–39.
[9] M. Gajda, J.A. Litwin, Z. Tabarowski, O. Zagolski, T. Cichocki, J.P. Timmermans, D. Adriaensen, Development of rat tibia innervation: colocalization of autonomic nerve fiber markers with growth-associated protein 43, Cells Tissues Organs 191 (2010) 489–499.
[10] R. Mirsky, A. Woodhoo, D.B. Parkinson, P. Arthur-Farraj, A. Bhaskaran, K.R. Jessen, Novel signals controlling embryonic Schwann cell development, myelination and dedifferentiation, J. Peripher. Nerv. Syst. 13 (2008) 122–135.
[11] S. Shibata, A. Yasuda, F. Renault-Mihara, S. Suyama, H. Katoh, T. Inoue, Y.U. Inoue, N. Nagoshi, M. Sato, M. Nakamura, C. Akazawa, H. Okano, Sox10-Venus mice: a new tool for real-time labeling of neural crest lineage cells and oligodendrocytes, Mol. Brain 3 (2010) 31.
[12] K.R. Jessen, R. Mirsky, The origin and development of glial cells in peripheral nerves, Nat. Rev. Neurosci. 6 (2005) 671–682.
[13] K. Tainaka, T.C. Murakami, E.A. Susaki, C. Shimizu, R. Saito, K. Takahashi, A. Hayashi-Takagi, H. Sekiya, Y. Arima, S. Nojima, M. Ikemura, T. Ushiku, Y. Shimizu, M. Murakami, K.F. Tanaka, M. Iino, H. Kasai, T. Sasaoka, K. Kobayashi, K. Miyazono, E. Morii, T. Isa, M. Fukayama, A. Kakita, H.R. Ueda, Chemical landscape for tissue clearing based on hydrophilic reagents, Cell Rep. 24 (2018) 2196–2210 (e9).
[14] T. Kawamoto, Use of a new adhesive film for the preparation of multi-purpose fresh-frozen sections from hard tissues, whole-animals, insects and plants, Arch. Histol. Cytol. 66 (2003) 123–143.
[15] B.D. Metscher, MicroCT for developmental biology: a versatile tool for high-contrast 3D imaging at histological resolutions, Dev. Dyn. 238 (2009) 632–640.
[16] S. Kanzaki, Y. Takada, S. Niida, Y. Takeda, N. Udagawa, K. Ogawa, N. Nango, A. Momose, K. Matsuo, Impaired vibration of auditory ossicles in osteopetrotic mice, Am. J. Pathol. 178 (2011) 1270–1278.
[17] R.E. Tomlinson, Z. Li, Q. Zhang, B.C. Goh, Z. Li, D.L.J. Thorek, L. Rajbhandari, T.M. Brushart, L. Minichiello, F. Zhou, A. Venkatesan, T.L. Clemens, NGF-TrkA signaling by sensory nerves coordinates the vascularization and ossification of developing Endochondral bone, Cell Rep. 16 (2016) 2723–2735.
[18] K.D. Shelbourne, M. Clark, T. Gray, Minimum 10-year follow-up of patients after an acute, isolated posterior cruciate ligament injury treated nonoperatively, Am. J. Sports Med. 41 (2013) 1526–1533.
[19] S. Kamekura, K. Hoshi, T. Shimoaka, U. Chung, H. Chikuda, T. Yamada, M. Uchida, N. Ogata, A. Seichi, K. Nakamura, H. Kawaguchi, Osteoarthritis development in novel experimental mouse models induced by knee joint instability, Osteoarthr. Cartil. 13 (2005) 632–641.
[20] K. Edoff, M. Grenegard, C. Hildebrand, Retrograde tracing and neuropeptide immunohistochemistry of sensory neurones projecting to the cartilaginous distal femoral epiphysis of young rats, Cell Tissue Res. 299 (2000) 193–200.
[21] J.J. Ivanusic, Size, neurochemistry, and segmental distribution of sensory neurons innervating the rat tibia, J. Comp. Neurol. 517 (2009) 276–283.
[22] W.M. Rogers, H. Gladstone, Vascular foramina and arterial supply of the distal end of the femur, J. Bone Joint Surg. Am. 32 (A) (1950) 867–874.
[23] M. Segarra, B.C. Kirchmaier, A. Acker-Palmer, A vascular perspective on neuronal migration, Mech. Dev. 138 (Pt 1) (2015) 17–25.
[24] T. Walchli, A. Wacker, K. Frei, L. Regli, M.E. Schwab, S.P. Hoerstrup, H. Gerhardt, B. Engelhardt, Wiring the vascular network with neural cues: a CNS perspective, Neuron 87 (2015) 271–296.
[25] D. Wang, F. Wu, H. Yuan, A. Wang, G.J. Kang, T. Truong, L. Chen, A.S. McCallion, X. Gong, S. Li, Sox10(+) cells contribute to vascular development in multiple organs-brief report, Arterioscler. Thromb. Vasc. Biol. 37 (2017) 1727–1731.
[26] P.L. Reno, W.E. Horton Jr., R.M. Elsey, C.O. Lovejoy, Growth plate formation and development in alligator and mouse metapodials: evolutionary and functional implications, J. Exp. Zool. B Mol. Dev. Evol. 308 (2007) 283–296.
[27] A.P. Kusumbe, S.K. Ramasamy, R.H. Adams, Coupling of angiogenesis and osteogenesis by a specific vessel subtype in bone, Nature 507 (2014) 323–328.
[28] K. Matsuo, Y. Kuroda, N. Nango, K. Shimoda, Y. Kubota, M. Ema, L. Bakiri, E.F. Wagner, Y. Takeda, W. Yashiro, A. Momose, Osteogenic capillaries orchestrate growth plate-independent ossification of the malleus, Development 142 (2015) 3912–3920.
[29] S.J. Sample, C.M. Heaton, M. Behan, J.A. Bleedorn, M.A. Racette, Z. Hao, P. Muir, Role of calcitonin gene-related peptide in functional adaptation of the skeleton, PLoS One 9 (2014) e113959.
[30] R.E. Tomlinson, Z. Li, Z. Li, L. Minichiello, R.C. Riddle, A. Venkatesan, T.L. Clemens, NGF-TrkA signaling in sensory nerves is required for skeletal adaptation to mechanical loads in mice, Proc. Natl. Acad. Sci. U. S. A. 114 (2017) E3632–E3641.
[31] M. Zaidi, T.J. Chambers, R.E. Gaines Das, H.R. Morris, I. MacIntyre, A direct action of human calcitonin gene-related peptide on isolated osteoclasts, J. Endocrinol. 115 (1987) 511–518.
[32] S.G. Grassel, The role of peripheral nerve fibers and their neurotransmitters in cartilage and bone physiology and pathophysiology, Arthritis Res. Ther. 16 (2014) 485.
[33] S. Imai, Y. Matsusue, Neuronal regulation of bone metabolism and anabolism: calcitonin gene-related peptide-, substance P-, and tyrosine hydroxylase-containing nerves and the bone, Microsc. Res. Tech. 58 (2002) 61–69.
[34] K. Irie, F. Hara-Irie, H. Ozawa, T. Yajima, Calcitonin gene-related peptide (CGRP)-containing nerve fibers in bone tissue and their involvement in bone remodeling, Microsc. Res. Tech. 58 (2002) 85–90.
[35] K. Aso, M. Izumi, N. Sugimura, Y. Okanoue, T. Ushida, M. Ikeuchi, Nociceptive phenotype alterations of dorsal root ganglia neurons innervating the subchondral bone in osteoarthritic rat knee joints, Osteoarthr. Cartil. 24 (2016) 1596–1603.
[36] M. Dirmeier, S. Capellino, T. Schubert, P. Angele, S. Anders, R.H. Straub, Lower density of synovial nerve fibres positive for calcitonin gene-related peptide relative to substance P in rheumatoid arthritis but not in osteoarthritis, Rheumatology (Oxford) 47 (2008) 36–40.